Quincke rotation driven flows

M. Belovs and A. Cēbers [*]

MMML Lab, Department of Physics, University of Latvia, Jelgavas-3, Rīga, LV-1004, Latvia

Flows induced by Quincke rotation in particle suspensions are considered. Nonlinear boundary problems for the suspension velocity and particle angular velocity fields in rectangular capillaries are formulated and solved for both no-slip and free boundary conditions. Linear stability analysis shows that the critical electric field strength necessary for the development of macroscopic flow is smaller than the field strength at which spontaneous Quincke rotation of a single particle occurs. This decrease is caused by hydrodynamic synchronization of the particle rotations. In the case of free boundaries interesting intermittent behavior is observed: as the parameters governing the problem pass degenerate eigenmodes revealed by the stability analysis, the nature of the induced flow changes qualitatively.

I. INTRODUCTION

Spontaneous rotation of dielectric particles in weakly conducting fluids was discovered by Quincke at the end of the 19th century [1]. The model of the Quincke effect in the frame of the leaky dielectric approach was developed in Ref. [2]. This model accounts for the action of antisymmetric stress and can therefore describe a wide variety of experimentally observed phenomena such as the collective motion of rolling Quincke particles [3], vortex flow in Quincke suspensions [4], and frictionless flow of the Quincke suspensions in capillaries under the action of an electric field [5]. The particle polarization equations initially derived for spherical particles were generalized to the case of ellipsoidal particles [6], leading to a description of the anomalous orientation perpendicular to the applied electric field [7,8]. It is interesting to note that including rotational inertia in the polarization model of leaky particles [2] leads to an exact derivation of the Lorentz equations and an experimental confirmation of deterministic chaos in the polarization model of leaky particles [9]. A rich class of phenomena has been observed for leaky droplets in an electric field, starting with the observation by Taylor that droplets deform into oblate shapes [10]. A substantial review of the electrohydrodynamics of droplets relevant to the Quincke effect is given in Ref. [11]. Among the different reviewed effects the equatorial streaming of the oblate droplets with the formation of sheets and their capillary breaking [12], the Quincke rotation of the droplets and formation of tilted configurations [13–15], and instabilities of particle belts leading to the formation of counter-rotating vortices on the equator of the Pickering droplets [16,17] should be mentioned. Recently, the Quincke effect in more complex situations was investigated. The Quincke particle with an attached flexible tail shows the Hopf bifurcation and self-propulsion due to the induced bending waves on the tail [18]. In Ref. [19] it is shown that a Quincke particle in the shape of a helix self-propels without the necessity for a solid wall as in the case of the Quincke rollers [3]. An algorithm for numerical simulation of the Quincke droplets based on the boundary integral equation technique is developed in Ref. [20].
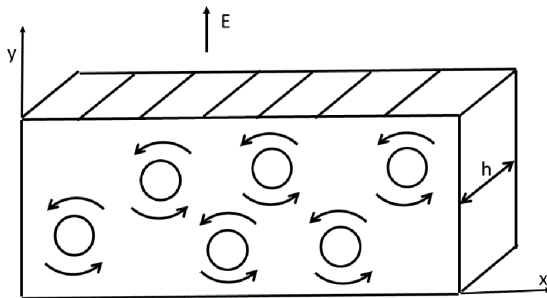
---

[*]aceb@tesla.sal.lv

FIG. 1. Sketch of rectangular capillary with a thickness h. Rotations of the particles in xy plane create the flow in the $\pm x$ direction [in the case of free boundaries (hatched)]. On hatched walls of the capillary nonslip (Sec. II A) or nonstress (Sec. II C) boundary conditions are applied.

Spontaneous rotation of the single Quincke particle occurs in a plane perpendicular to the applied electric field, but its direction is undetermined. In Ref. [21] the probability distribution function of particle rotation planes is introduced, and it is shown that due to the induced flow the particle rotation planes are ordered if the particle concentration is sufficiently large. In Ref. [22] this model is applied for smoothing the velocity profiles of the capillary flow of the Quincke suspension predicted by simple models [23].

Here, motivated by the results of Ref. [21], we consider the flow induced by rotating Quincke particles in some simple geometries. The density-matched suspension is considered, and electric interactions between the particles and with walls of capillary are neglected. Since the densities of particles and fluid are matched, particles do not sediment on the capillary walls, and their rolling motion [3] is not important.

II. CAPILLARY FLOW

A. Capillary flow at nonslip boundary conditions

Let us consider a rectangular capillary with the x axis along its long side, the y axis along its short side, and the z axis perpendicular to the boundaries of the capillary (Fig. 1). The friction with the walls is accounted for in the Brinkman approximation. Since the rotations of particles are synchronized by the flow as shown in Ref. [21] the angular velocity has only a z component. The set of equations describing the flow and the rotation of the particles in the stationary case includes the equation of fluid motion in the inertialess Brinkman approximation accounting for volume torque due to the particles rotating with the angular velocity $\vec{\Omega}$ with respect to the fluid, where the angular velocity is $\vec{\Omega}_0 = 1/2 \vec{\nabla} \times \vec{v}$. β takes into account the friction of the liquid with the side walls of capillary and may be estimated according to the relation $\beta = 12\eta/h^2$ (h is the thickness of the capillary),

$$-\vec{\nabla}p + \eta\Delta\vec{v} + \tfrac{1}{2}\vec{\nabla} \times \alpha(\vec{\Omega} - \vec{\Omega}_0) - \beta\vec{v} = 0, \tag{1}$$

the torque balance on the particles, which includes the torque due to the electric field, the friction with the liquid, and the couple stress due to the diffusion of the angular momentum

$$\vec{P} \times \vec{E} - \alpha(\vec{\Omega} - \vec{\Omega}_0) + D\Delta\vec{\Omega} = 0, \tag{2}$$

and the polarization relaxation equation in the stationary case,

$$\vec{\Omega} \times \vec{P} - \frac{1}{\tau}(\vec{P} - \chi\vec{E}) = 0. \tag{3}$$

Here α is the rotational drag coefficient, $\vec{\Omega}_0 = \frac{1}{2}\vec{\nabla} \times \vec{v}$, τ is the Maxwell polarization relaxation time, and $\chi = \chi_0 - \chi_\infty$ is the polarizability of the spherical particle with the radius a, which depends on the dielectric permeabilities and the conductivities of the particle and the surrounding liquid according to $\chi_0 = 4\pi\varepsilon_1 a^3(\gamma_2 - \gamma_1)/(\gamma_2 + 2\gamma_1)$, $\chi_\infty = 4\pi\varepsilon_1 a^3(\varepsilon_2 - \varepsilon_1)/(\varepsilon_2 + 2\varepsilon_1)$, where indices 1 and 2 denote the electrophysical properties of the liquid and particles, respectively [2]. The polarizability of the Quincke particles $\chi < 0$ and their spontaneous rotation occurs in the electric field $E > E_c$ (E_c is the critical electric field strength at which the supercritical bifurcation of the angular velocity of the single Quincke particle in the quiescent fluid arises and is given by the relation [2] $E_c^2 = -\alpha/\tau\chi$). Due to the negative effective viscosity of the Quincke suspension multilayer structure of the velocity profiles arises. To resolve the boundary layers between different domains of the fluid motion the spin diffusion coefficient D is introduced similarly as is done, for example, in Ref. [24] when considering the boundary layer of the edge flow in the system of active spinners. An interesting feature of the model is that due to the cooperative rotation effect the macroscopic flow arises even at $E < E_c$ [21]. Here we may remark on the following. In Ref. [25] data of the effective viscosity measurements of the Quincke suspension in the Couette rheometer are given for $E \geqslant E_c$, which show a decrease of the effective viscosity with the shear rate (no data are given for $E < E_c$). Since the calculation shows that a similar effect persists also for $E < E_c$, then we may conclude that the experimental data in Ref. [25] indirectly confirm the decrease of the critical field for the suspension in comparison with a single particle. This is illustrated by finding the nontrivial solution $\vec{v} = (v(y), 0, 0)$, $\vec{\Omega} = (0, 0, \Omega)$ of the nonlinear boundary problem [Eqs. (1)–(3)] at $0 < y < d$:

$$\frac{d^2v}{dy^2} + \frac{2a}{1+a}\frac{d\Omega}{dy} - \frac{d^2}{l_v^2}v = 0\,, \tag{4}$$

$$\varepsilon\frac{d^2\Omega}{dy^2} = \Omega - \frac{\Omega}{1+\Omega^2}\frac{E^2}{E_c^2} + \frac{1}{2}\frac{dv}{dy} \tag{5}$$

with boundary conditions

$$v|_{y=0,1} = 0, \quad \left.\frac{d\Omega}{dy}\right|_{y=0,1} = 0. \tag{6}$$

Here the velocity of the flow is scaled by d/τ, the angular velocity by $1/\tau$, and y by the width of the capillary d. The following notations are introduced: $l_v^2 = (\eta + \alpha/4)/\beta$, $l_\Omega^2 = D/\alpha$, $\varepsilon = l_\Omega^2/d^2$, $a = \alpha/(4\eta)$, and $b^2 = a/(1+a)$.

Neutral solutions of the linear problem are found by linearizing Eq. (5). The critical values of E_n^2/E_c^2 for eigenmode n $(v, \Omega) \sim (\sin(n\pi y), \cos(n\pi y))$ may be found analytically, yielding

$$\frac{E_n^2}{E_c^2} = 1 + \frac{b^2 l_v^2 n^2 \pi^2}{d^2}\left(w^2 - \frac{1}{1 + l_v^2 n^2 \pi^2/d^2}\right). \tag{7}$$

The minimal value of the critical electric field $\min_n(E_n^2/E_c^2) = 1 - b^2(1-w)^2$ $(w^2 = l_\Omega^2/l_v^2 b^2$, $b^2 = a/1+a)$ corresponds to $\varepsilon n^2\pi^2 = b^2 w(1-w)$ and is less than 1 for $w \in (0, 1)$.

The first few linear instability modes $(n = 1, \ldots, 4)$ are shown in Fig. 2 for $w = 0.1$ and $1 - E^2/E_c^2 = 0.81b^2$. The critical ε values of the modes are given by the relation $\varepsilon_c(n)/b^2 = w(1-w)/n^2\pi^2$. We see that for the higher modes the critical diffusion length of the angular velocity is comparatively smaller at given electric field strength. This illustrates the regularizing role of the internal angular momentum diffusion. The velocity and angular velocity profiles for the second mode are shown in Fig. 3. The linear stability neutral modes we have obtained enable us to efficiently find the solutions of the nonlinear boundary problem using the MATLAB routine bvp4c. Figure 4 shows solutions for the velocity and angular velocity fields corresponding to the development of the second mode of the linear instability for several values of the electric field above the critical value $1 - E^2/E_c^2 = (0.5, 0.6, 0.7)b^2$. The mechanism behind the induced flow
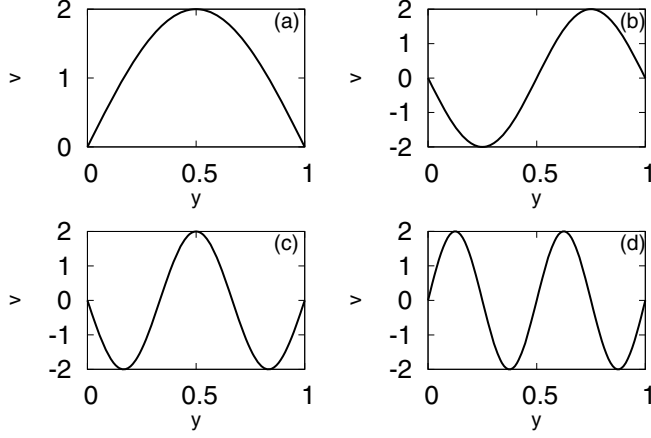
FIG. 2. Neutral modes at nonslip boundary conditions. $1 - E^2/E_c^2 = 0.81b^2$, $w = 0.1$. (a) ($n = 1$), (b) ($n = 2$), (c) ($n = 3$), (d) ($n = 4$).

may be easily explained by considering the angular velocity distribution. As shown in Fig. 4(b) the particles rotate counterclockwise for $y < 0.25$, $y > 0.75$ and clockwise for $0.25 < y < 0.75$. The force due to the nonuniform angular velocity field pushes the liquid in the negative x axis direction for $0 < y < 0.5$ and the positive x axis direction for $0.5 < y < 1$ as shown in Fig. 4(a).

The Poiseuille-like mode [see Fig. 2(a)] has been experimentally observed in a density-matched Quincke suspension as described in Ref. [25]. We should remark that in Ref. [25] it is noted that the simple model with internal rotations does not work at small shear rates when the effective viscosity in the field is even greater than at zero field. The clarification of this behavior is given in the authors' previous work [26], where the picture of particle layers perpendicular to the vorticity of the flow is shown. We believe that the formation of such layering is due to the dipolar interaction of rotating particles, which is not taken into account by the model (1)–(3). We may remark that the formation of the similar multilayer structure of the suspension of magnetic particles in a rotating field was considered in Ref. [27].

B. Vortex flow

The mechanism we have described for inducing macroscopic flow by inhomogeneous particle rotations causes vortex-like flow in axisymmetric conditions when the Quincke suspension is between two disks with radius R at a distance $2d$ (Fig. 5). Looking for the neutral solution of the velocity field as $\vec{v} = (0, v_\varphi(r)\frac{d^2-z^2}{d^2}, 0)$, $\vec{\Omega}_0 = \frac{1}{2}\{\frac{2v_\varphi(r)z}{d^2}, 0, \frac{1}{r}\frac{d}{dr}[rv_\varphi(r)]\frac{d^2-z^2}{d^2}\}$ Eq. (3) up to the first-order terms in the velocity of flow yields the following expression for the azimuthal force
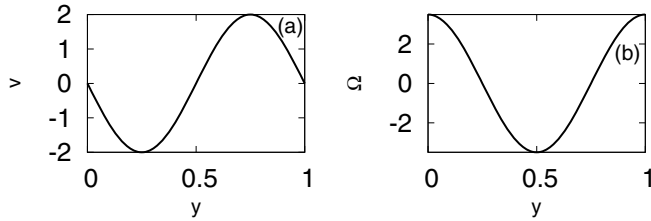

FIG. 3. Velocity (a) and angular velocity (b) profiles for second neutral mode; $1 - E^2/E_c^2 = 0.81b^2$, $w = 0.1$.
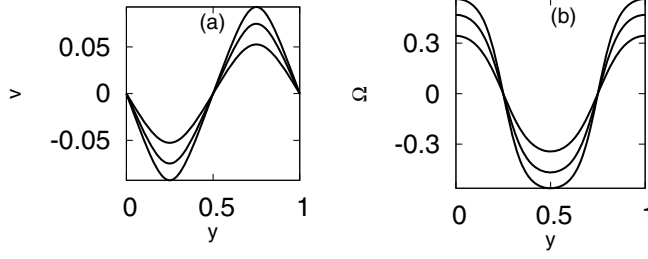
FIG. 4. Velocity (a) and angular velocity (b) profiles as solutions of nonlinear boundary problem. From down to up, $1 - E^2/E_c^2 = (0.5, 0.6, 0.7)b^2$, $\varepsilon = b^2 w(1-w)/4\pi^2$, $a = 1$, $w = 0.1$.

acting on the liquid: $\frac{1}{2}[\vec{\nabla} \times (\vec{P}_1 \times \vec{E})]_\varphi = \frac{\alpha}{2} \frac{E^2/E_c^2}{1-E^2/E_c^2} \frac{v_\varphi}{d^2}$. As a result we obtain an equation for the mean velocity (averaged across the thickness of the layer) $\langle v_\varphi \rangle$ ($\langle v_\varphi \rangle = 2v_\varphi/3$),

$$\eta\left(\frac{d^2\langle v_\varphi \rangle}{dr^2} + \frac{1}{r}\frac{d\langle v_\varphi \rangle}{dr} - \frac{\langle v_\varphi \rangle}{r^2}\right) + \beta\langle v_\varphi \rangle = 0\,, \tag{8}$$

where

$$\beta = -\frac{3}{d^2}\left(\eta - \frac{\alpha}{4}\frac{E^2/E_c^2}{1-E^2/E_c^2}\right). \tag{9}$$

We see that contrary to the usual case β may be positive at $E^2/E_c^2 > 1/(1 + \alpha/4\eta)$. This is the negative viscosity effect of the Quincke suspension [6].

The nontrivial solutions of Eq. (8) assuming a no-slip boundary condition at $r = R$ are $\langle v_\varphi \rangle \sim J_1(\gamma_n r/R)$, where J_1 is the Bessel function and γ_n is nth root of the Bessel function. The critical electric field for the growth of nth vortex mode satisfies the relation

$$1 - \frac{E^2}{E_c^2} = \frac{\alpha}{4\eta + \alpha + 4\eta\gamma_n^2 d^2/3R^2}. \tag{10}$$

The lowest critical value of E^2/E_c^2 corresponds to $n = 1$, and the corresponding mode is shown in Fig. 6.

C. Capillary flow with free interfaces

An important aspect of the flow induced by the internal rotations is the edge effect at the free interfaces [4,28–30]. To illustrate this, let us consider a simple model that does not take into account
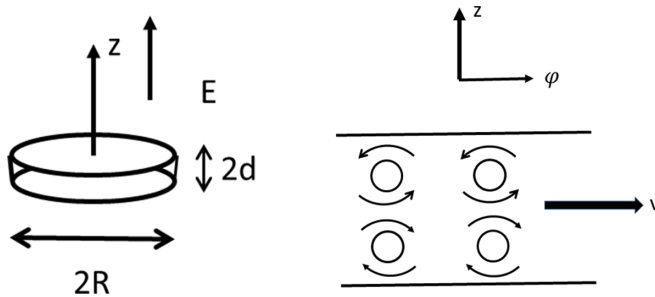

FIG. 5. The vortex flow of the Quincke suspension is created by nonhomogeneous rotations of the particles in the cross section of the capillary as shown on the right side.
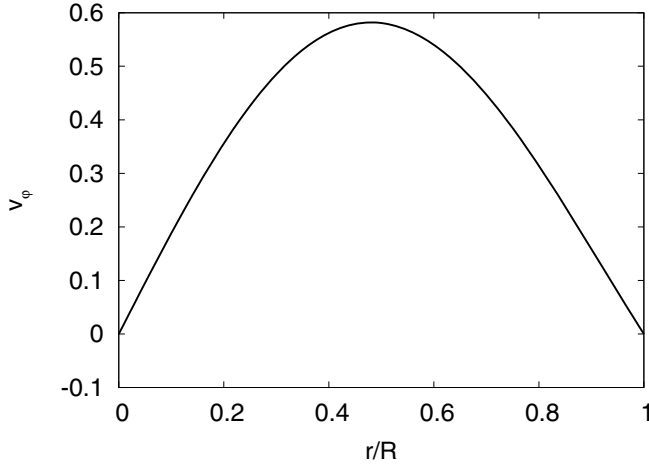
FIG. 6. Velocity profile of vortex flow.

the couple stress in Eqs. (1)–(3). The flow is defined by the velocity field $\vec{v} = (v(y), 0, 0)$ and the angular velocity $\vec{\Omega} = (0, 0, \Omega)$. At the free boundary the condition of zero stress is in effect

$$\sigma = \eta \frac{dv}{dy} + \frac{\alpha}{2}(\Omega - \Omega_0) = 0, \tag{11}$$

which yields $v = 2\alpha\Omega y/(4\eta + \alpha)$, where the angular velocity Ω can be determined from the equation as follows from Eqs. (2) and (3):

$$\frac{\tau\Omega}{1 + (\tau\Omega)^2} \frac{E^2}{E_c^2} - \tau\Omega \frac{4\eta}{\alpha + 4\eta} = 0, \tag{12}$$

which has a nontrivial solution at $E^2 > E_{c*}^2$, where

$$E_{c*}^2 = E_c^2/(1 + \alpha/4\eta). \tag{13}$$

Thus, the critical field strength required for the flow pattern to develop is below the field strength at which spontaneous rotations of individual particles arise due to the cooperative hydrodynamic interaction between the particles.

The nonlinear boundary problem for the layer with free boundaries at zero stress and couple stress on the free boundaries in the same notations as used before reads

$$\frac{d^2 v}{dy^2} + \frac{2a}{1 + a}\frac{d\Omega}{dy} - \frac{d^2}{l_v^2}v = 0, \tag{14}$$

$$\varepsilon \frac{d^2\Omega}{dy^2} = \Omega - \frac{\Omega}{1 + \Omega^2}\frac{E^2}{E_c^2} + \frac{1}{2}\frac{dv}{dy}, \tag{15}$$

with boundary conditions

$$\left(\frac{dv}{dy} + \frac{2a}{1 + a}\Omega\right)\bigg|_{y=\pm1} = 0, \quad \frac{d\Omega}{dy}\bigg|_{y=\pm1} = 0. \tag{16}$$

The problem (14)–(16) has a number of interesting properties. To illustrate this, we regard the boundary problem for the neutral perturbations of the linear stability problem as an eigenvalue problem for the critical electric field strength required for the induced flow. The resulting neutral
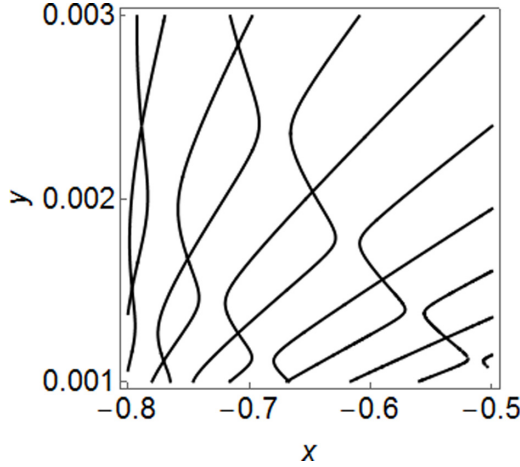
FIG. 7. Neutral curves of layer with free boundaries ($w = 0.1$): $y = \varepsilon/b^2$, $x = (E^2/E_c^2 - 1)/b^2$.

curves are shown in Fig. 7 for particular value $w \in (0; 1)$ ($\frac{\varepsilon d^2}{b^2 l_v^2} = 0.01$). For large values of the parameter ε the critical value of the electric field strength corresponds to that given by relation (13) and is the sole neutral mode for $E^2/E_c^2 < 1$. If $w < 1$ as the parameter ε is decreased the higher modes of the velocity profile corresponding to $-1 < (E^2/E_c^2 - 1)/b^2 < 0$ appear when the neutral curves cross $E^2/E_c^2 = 1$. The first mode corresponding to the Poiseuille-like velocity profile (as shown by the solution of the corresponding eigenvalue problem) appears at $\varepsilon/b^2 = 4[1 - z/\tan(z)]/(2z)^2$, where z is determined by the relation $w^2 = z/\tan(z)$. The corresponding relations may also be derived for higher modes. For small values of the parameter ε there are many modes at $w \in (0, 1)$ corresponding to $(E^2/E_c^2 - 1)/b^2 < 0$ as may be seen in Fig. 7.

The intersections of curves shown in Fig. 7 correspond to the degeneracy of eigenmodes. The first two modes seen on the left side of Fig. 7 correspond to linear (Couette-like) and parabolic (Poiseuille-like) velocity profiles. The corresponding velocity profiles slightly above the degeneracy point are shown in Figs. 8(a) and 8(b) [$\varepsilon/b^2 = 0.0279$, $(E^2/E_c^2 - 1)/b^2 = -0.905$]. At the degeneracy point the modes are similar to edge solutions at $y = -1$ or $y = 1$ (Fig. 9). Passing the degeneracy point the neutral modes interchange and the dominant mode until the next degeneracy point (see Fig. 8) is the Poiseuille-like mode. The first intersection ($k = 1$) of neutral curves corresponding to the Couette-like and Poiseuille-like modes may be found by rather complex analytical calculations, which give

$$\left(\frac{E^2}{E_c^2} - 1\right)/b^2 = -1 + \frac{2w}{w + \sqrt{4 + w^2}} \tag{17}$$
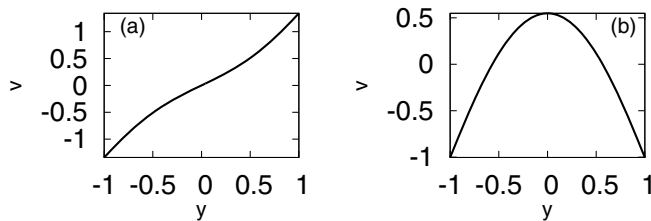

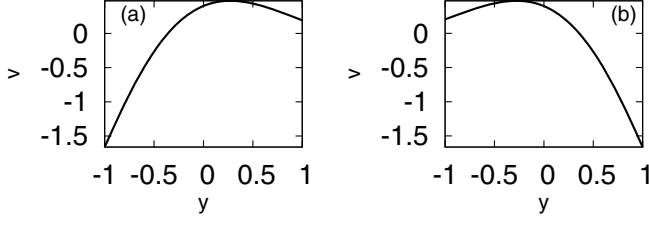FIG. 8. Velocity profiles of two first modes. $w = 0.1$, $\varepsilon/b^2 = 0.0279$, $(E^2/E_c^2 - 1)/b^2 = -0.905$.

FIG. 9. Neutral modes at point of degeneracy. $E^2/E_c^2 - 1)/b^2 = -0.9049$, $\varepsilon/b^2 = 0.0279$ as calculated according the relations (17) and (18) for $w = 0.1$.

and (k is number of intersection)

$$\frac{\varepsilon}{b^2} = \frac{w}{2\pi^2 k^2}(3\sqrt{4 + w^2} - 5w). \tag{18}$$

The situation is even more interesting at $w > 1$. In this case for $(E^2/E_c^2 - 1)/b^2 \in (-1, 0)$ only one or two modes exist. The first corresponds to the Couette-like velocity profile and exists for all values ε. The second mode corresponding to the Poiseuille-like velocity profile appears at the critical parameter ε value given by the relation $\varepsilon/b^2 = 4[z/\tanh(z) - 1]/(2z)^2$, where z is determined by the relation $w^2 = z/\tanh(z)$. There we see the intersection of the neutral curves of these two modes. The velocity profile corresponding to the intersection point at $w = 2.1$: $\varepsilon/b^2 = 0.026$, $(E^2/E_c^2 - 1)/b^2 = -0.157$, is shown in Fig. 10. A pronounced edge mode character may be seen. Edge flows have been seen experimentally in different systems. For instance, in a suspension of hematite cubes in a horizontal rotating magnetic field, edgelike particle motion is observed in Ref. [29]. Similar phenomena are seen in Ref. [30] in the suspension of Janus magnetic particles in the rotating field where their rotation is driven by the anisotropy of magnetic susceptibility.

The solutions of the nonlinear boundary problem (14)–(16) for several values of the viscous penetration length using the MATLAB subroutine bvp4c are shown in Fig. 11. The characteristic edgelike motion driven by the internal rotations near the free interfaces may be observed. For smaller values of l_v it competes with the flow caused by the nonuniform particle rotations.
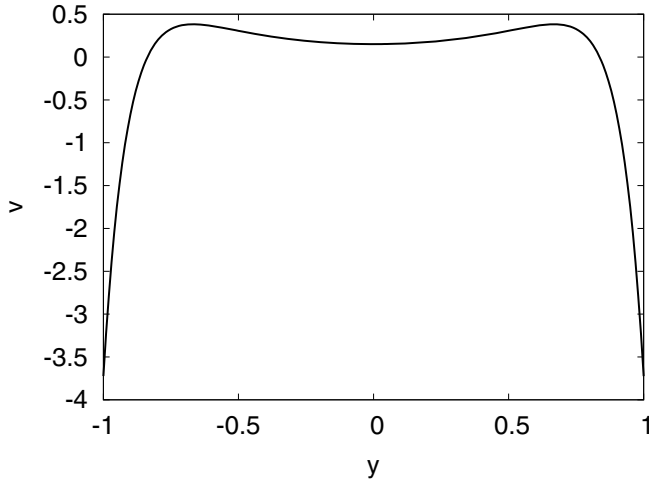

FIG. 10. Velocity profile of the normalized neutral mode at the degeneracy point corresponding to $w = 2.1$, $\varepsilon/b^2 = 0.025$, $(E^2/E_c^2 - 1)/b^2 = -0.157$. Pronounced edgelike flow is present.
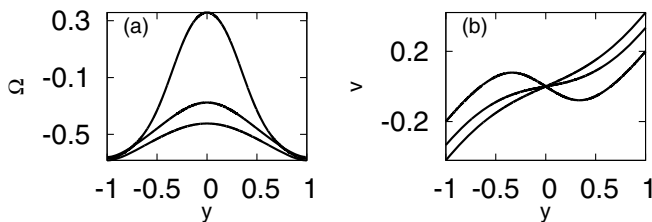
FIG. 11. Solutions of the nonlinear boundary problem Eqs. (14)–(16) for the velocity and angular velocity profiles for several values of the viscous penetration length l_v. Flatter profiles correspond to a larger viscous penetration length. $E^2/E_c^2 = 0.8$, $\varepsilon = 0.01$, $a = 1$, $d^2/l_v^2 = (1, 1.5, 2)$. d^2/l_v^2 increases from down to up.

III. CONCLUSIONS

Properties of flows in rectangular capillaries caused by the inhomogeneous rotations of Quincke particles are analyzed at no-slip and free boundary conditions. By linearizing the nonlinear boundary problems the conditions for the development of the suspension flow without applying any external forces are obtained. It is found that the critical electric field for the development of the macroscopic flow is less than the critical electric field at which a spontaneous rotation of a single Quincke particles arises. This illustrates the synchronization of particle rotations by the flow. In the axisymmetric geometry, the critical electric field strength for the development of the vortex flow is found. In the case of the flow with the free boundaries the typical feature is the development of the edge flows.

ACKNOWLEDGMENT

---

[1] G. Quincke, Ueber Rotationen im constanten elektrischen Felde, Ann. Phys. Chem. **59**, 417 (1896).

[2] A. O. Tsebers, Internal rotations in the hydrodynamics of conducting dielectric suspensions, Fluid Dyn. **15**, 245 (1980).

[3] A. Bricard, J.-B. Coussin, N. Desreumax, O. Dauchot, and D. Bartolo, Emergence of macroscopic directed motion in population of motile colloids, Nature (London) **503**, 95 (2013).

[4] A. Bricard, J.-B. Coussin, D. Das, Ch. Savoie, V. Chikkodi, K. Shitara, O. Chepizhko, F. Peruani, D. Saintillan, and D. Bartolo, Emergent vortices in populations of colloidal rollers, Nat. Commun. **6**, 7470 (2018).

[5] A. Cebers, E. Lemaire, and L. Lobry, Flow modification induced by Quincke rotation in a capillary, Int. Journ. Mod. Phys. **16**, 2603 (2002).

[6] A. O. Tsebers, Electrohydrodynamic instabilities in weakly conducting suspension of ellipsoidal particles, Magnetohydrodynamics **16**, 175 (1980).

[7] A. Cebers, E. Lemaire, and L. Lobry, Electrohydrodynamic instabilities and orientation of dielectric ellipsoids in low-conducting fluids, Phys. Rev. E **63**, 016301 (2001).

[8] Q. Brosseau, G. Hickey, and P. M. Vlahovska, Electrohydrodynamic Quincke rotation of an ellipsoid, Phys. Rev. Fluids **2**, 014101 (2017).

[9] E. Lemaire and L. Lobry, Chaotic behavior in electro-rotation, Physica A **314**, 663 (2002).

[10] G. I. Taylor, The circulation produced in a drop by an electric field, Proc. Roy. Soc. A **291**, 159 (1966).

[11] P. M. Vlahovska, Electrohydrodynamics of drops and vesicles, Ann. Rev. Fluid Mech. **51**, 305 (2019).

[12] Q. Brosseau and P. M. Vlahovska, Streaming from the Equator of a Drop in an External Electric Field, Phys. Rev. Lett. **119**, 034501 (2017).

[13] M. Ouriemi and P. M. Vlahovska, Electrohydrodynamic deformation and rotation of a particle-coated drop, Langmuir **31**, 6298 (2015).

[14] P.-F. Salipante and P. M. Vlahovska, Electrohydrodynamic rotations of a viscous droplet, Phys. Rev. E **88**, 043003 (2013).

[15] P. F. Salipante and P. M. Vlahovska, Electrohydrodynamics of drops in strong uniform dc electric fields, Phys. Fluids **22**, 112110 (2010).

[16] P. Dommersnes, Z. Rozynek, K. Mikkelsen, R. Castberg, K. Kjerstad, K. Nersvil, and J. O. Fossum, Active structuring of colloidal armour on liquid drops, Nat. Commun. **4**, 2066 (2013).

[17] M. Ouriemi and P. M. Vlahovska, Electrohydrodynamics of particle-covered drops, J. Fluid Mech. **751**, 106 (2014).

[18] L. Zhu and H. A. Stone, Propulsion driven by self-oscillation via an electrohydrodynamic instability, Phys. Rev. Fluids **4**, 061701(R) (2019).

[19] D. Das and E. Lauga, Active Particles Powered by Quincke Rotation in a Bulk Fluid, Phys. Rev. Lett. **122**, 194503 (2019).

[20] D. Das and D. Saintillan, Electrohydrodynamics of viscous drops in strong electric fields: Numerical simulation, J. Fluid Mech. **829**, 127 (2017).

[21] M. Belovs and A. Cebers, Relaxation of polar order in suspensions with Quincke effect, Phys. Rev. E **89**, 052310 (2014).

[22] A. Cebers, Poiseuille flow of a Quincke suspension, Phys. Rev. E **90**, 032305 (2014).

[23] H.-F. Huang, M. Zahn, and E. Lemaire, Continuum modeling of micro-particle electrorotation in Couette and Poiseuille flows—The zero spin viscosity limit, J. Electrostatics **68**, 345 (2010).

[24] B. C. Van Zuiden, J. Paulose, W. T. M. Irvine, D. Bartolo, and V. Vitelli, Spatiotemporal order and emergent edge currents in active spinner materials, Proc. Natl. Acad. Sci. USA **113**, 12919 (2016).

[25] F. Peters, L. Lobry, and E. Lemaire, Pressure-driven flow of a micropolar fluid: Measurement of the velocity profile, J. Rheol. **54**, 311 (2010).

[26] N. Pannaci, E. Lemaire, and L. Lobry, Rheology and structure of a suspension of particles subjected to Quincke rotation, Rheol. Acta **46**, 899 (2007).

[27] G. Bossis and A. Cebers, Effects of the magnetodipolar interactions in the alternating magnetic fields, J. Magn. Magn. Mater. **201**, 218 (1999).

[28] A. O. Tsebers, Interfacial stresses in the hydrodynamics of liquids with internal rotation, Magnetohydrodynamics **11**, 63 (1975).

[29] V. Soni, E. Bililign, S. Magkiriaden, S. Sacanna, D. Bartolo, M. J. Shelley, and W. T. M. Itvine, The odd free-surface flows of a colloidal chiral fluid, Nat. Phys. **15**, 1188 (2019).

[30] J. Yan, S. C. Bae, and S. Granick, Rotating crystals of magnetic Janus colloids, Soft Matter **11**, 147 (2015).